



Elevated temperature evaluation of an existing steel web shear buckling analytical model



Maria E. Moreyra Garlock, Jonathan D. Glassman

Department of Civil and Environmental Engineering, Princeton University, United States

ARTICLE INFO

Article history:

Received 15 October 2013

Accepted 30 May 2014

Available online 1 July 2014

Keywords:

Nonlinear finite element analysis

Steel girder bridge

Postbuckling

Web shear buckling

Elevated temperatures

Fire

ABSTRACT

Steel plate girders with slender webs are particularly susceptible to severe damage when subjected to high temperatures due to fire. Using nonlinear finite element (FE) models, this study examines the buckling strength of steel plate girder webs subject to fire temperatures. The models were validated with experimental results presented by other researchers, and the validation study resulted in recommendations for appropriate FE representations of material properties and boundary conditions. The elastic shear buckling stress (τ_{cr}) and ultimate shear buckling stress (τ_u) was then studied for web plates with various span-to-depth (a/D) ratios and a range of temperatures representing fire conditions. The results of this parametric study were compared to predictions given by the Basler–Thürlimann (BT) closed-form solution, which was originally developed to predict τ_u at ambient temperature. Various representations of the elevated temperature stress, at the time of τ_u , were used in the BT solution and compared to the FE results. It was found that the BT solution provides adequate predictions of τ_u at elevated temperatures with appropriate substitutions for the yield stress.

© 2014 Elsevier Ltd. All rights reserved.

1. Introduction

Structural members composed of steel plates are potentially susceptible to web shear buckling, depending on the slenderness ratio, D/t_w , where D is the depth and t_w is the thickness of the web plate. Typically, web shear buckling is of particular concern for deep structures such as plate girder bridges and buildings with deep plate girders used for long spans or to transfer columns. For both structures, the accuracy of existing analytical tools for calculating postbuckling shear strength at elevated temperatures must be studied to determine the vulnerability of these structural systems to web shear buckling during a fire.

In the example of bridge structures, historical events show that fires pose a significant hazard to highway bridges. Data collected by the New York Department of Transportation (NYDOT) from voluntary submissions of 18 US states found that of the total recorded bridge failures up to and including the year 2011, 53 were due to fire compared to 18 due to earthquakes (seismically active states like California participated in the study) [1,2]. The primary cause of bridge fires is vehicular accidents occurring beneath or adjacent to the bridge. The most devastating of these fires are caused by accidents involving tanker trucks, whose large volume of combustible fuel can cause severe damage or collapse of nearby highway bridges (Fig. 1). Known as liquid pool fires, they

can result in steel temperatures exceeding 1000 °C [3]. Should any fuel leak from a damaged fuel tank and spread across the roadway, this would only lead to an increase in the energy output of the liquid pool fire and a larger fire load on the structure [4].

This hazard to highway bridges in particular is only compounded by the lack of fire design guidelines and post-fire strength assessment schemes [1,5]. The National Fire Protection Association (NFPA) requires the consideration of high temperature loading for bridge design. NFPA 502: Standard for Road Tunnels, Bridges, and Other Limited Access Highways requires a water standpipe system for situations where the distance to a water supply exceeds 122 m (Section 6.5), and also requires critical structural elements to protect from collision and high temperature loading (Section 6.5) [6]. Despite these requirements, the engineer receives no guidance regarding how to design a bridge that withstands high temperature loading, nor how to assess the post-fire strength of a bridge that has been damaged.

In contrast to bridges, building fires are fueled by paper, draperies, and home or office furnishings [7]. Further, buildings have combinations of active and passive fire resistance. Fire sprinklers (active) activate automatically in the event of a fire, while thermal insulation (passive) shields steel members from excessive heating. Fire is often a “secondary” event where the primary initiating event may be an earthquake, blast, or impact. This primary event may render the active and passive fire protection inoperable. Therefore, for important structural elements, such as a deep girder supporting many loads, a fundamental understanding of their response under fire conditions is important.

A literature review of relevant research has shown extensive experimental and FE studies of web shear buckling at ambient temperatures

E-mail addresses: mgarlock@princeton.edu (M.E.M. Garlock), jdglassm@princeton.edu (J.D. Glassman).



Fig. 1. I-20/I-59/I-65 interchange in Birmingham, AL after a fire: (a) severe deflections in the steel girders, and (b) web shear buckling observed near the bent cap. Photos courtesy of the Alabama DOT.

(summary provided in [8]). Elevated temperature experimental and FE studies were conducted at Nanyang Technological University in Singapore on small-scale plate girders, the results of which are discussed in Section 3 [9,10]. This paper differs from previous research since the web plates studied are deeper than that of previous research and are representative of bridges in service. Further, this paper examines the effects of material properties at elevated temperatures on the development of tensile stresses within the web at ultimate shear buckling.

The objective of this current study is to determine if an existing closed-form solution (developed for ambient temperature) for determining the ultimate shear buckling stress, τ_u , of a steel web plate is applicable at elevated temperatures. To accomplish this, τ_u values from the closed-form solution were compared with those from finite element (FE) analysis using the software Abaqus [11] for temperatures between 20 °C and 1100 °C. These FE models were based on the 1982 Standard Plans prepared by the Federal Highway Administration (FHWA) [12]. The FE models were validated with experimental data published by other researchers. This work will benefit engineers in evaluating the strength of steel plate girders in fire conditions.

2. Background

2.1. Elastic shear buckling at ambient temperature

To calculate the elastic critical buckling stress, τ_{cr} , of a rectangular plate subjected to pure shear loading, the following equation can be used [13]:

$$\tau_{cr} = k \frac{\pi^2 E}{12(1-\nu^2) \left(\frac{D}{t_w}\right)^2} \quad (1)$$

where E is Young's modulus, ν is Poisson's ratio, D is the depth of the plate, t_w is the plate thickness, and k is the elastic shear buckling coefficient. The value of k is a function of the span-to-depth ratio (a/D) of the plate and the boundary conditions supplied to its edges. When transverse stiffeners are used, a represents the centerline spacing between the stiffeners. D/t_w is the slenderness ratio and indicates how susceptible the girder is to web shear buckling. The elastic critical shear buckling load, V_{cr} , is calculated by multiplying Eq. (1) by Dt_w .

For a plate that is simply supported on all four edges, the elastic shear buckling coefficient, k_{ss} , is calculated as [13–15]:

$$k_{ss} = 4.00 + \frac{5.34}{\left(\frac{a}{D}\right)^2} \text{ for } a/D < 1 \quad (2a)$$

$$k_{ss} = 5.34 + \frac{4.00}{\left(\frac{a}{D}\right)^2} \text{ for } a/D \geq 1 \quad (2b)$$

For a plate that is simply supported on two opposing sides and fixed on the remaining two sides, the elastic shear buckling coefficient, k_{sf} , is calculated as [13–15]:

$$k_{sf} = \frac{5.34}{\left(\frac{a}{D}\right)^2} + \frac{2.31}{\left(\frac{a}{D}\right)} - 3.44 + 8.39\left(\frac{a}{D}\right) \text{ for } a/D < 1 \quad (3a)$$

$$k_{sf} = 8.98 + \frac{5.61}{\left(\frac{a}{D}\right)^2} - \frac{1.99}{\left(\frac{a}{D}\right)^3} \text{ for } a/D \geq 1 \quad (3b)$$

Transverse stiffeners are typically designed to provide simple support to the web and are idealized as such [15]. The web-flange juncture realistically offers support to the web plate that exists somewhere between a simple and fixed support. Various authors have elected to idealize this web-flange juncture as simply supported, fixed, or half of full fixity [8]. In the 1990s, finite element investigations were used to develop a more robust means of characterizing the edge support at the web-flange juncture by interpolating the value for the k coefficient between the calculated values of k_{ss} and k_{sf} depending on the flange-thickness-to-web-thickness ratio, t_f/t_w [14,15]. Thus, the value of k may be computed as:

$$k = k_{ss} + \frac{4}{5} (k_{sf} - k_{ss}) \left[1 - \frac{2}{3} \left(2 - \frac{t_f}{t_w} \right) \right] \text{ for } \frac{1}{2} \leq t_f/t_w < 2 \quad (4a)$$

$$k = k_{ss} + \frac{4}{5} (k_{sf} - k_{ss}) \text{ for } t_f/t_w \geq 2 \quad (4b)$$

2.2. Ultimate shear buckling at ambient temperature

Various theories have been developed to compute the ultimate shear buckling stress, τ_u , of plate girder webs by accounting for the postbuckling strength reserve for thin, rectangular plates loaded in shear [8]. The theories discussed in [8] are based on the fundamental assumption formulated through Wagner's 1931 published work, which states that compressive stresses in the direction perpendicular to the observed diagonal tension field do not increase once the elastic critical buckling strength has been reached [16,17]. By accepting this assumption, the subsequent tension field theories based the postbuckling strength of the web on the additional amount of tension that can be developed in the diagonal tension field.

The tension field theory proposed by Basler, which serves as the basis of the AASHTO LRFD Bridge Design Specifications [18] and is notable for balancing ease of use with accuracy [19], was selected as the analytical model against which to compare the finite element results to be discussed later. Basler's work published in the early 1960s offered the first postbuckling strength theory for steel plate girder webs [8,20]. In developing his model, Basler assumed that the flanges were too flexible

to provide anchorage for the horizontal component of the tension field and instead relied on the transverse stiffeners to develop axial compression [16,20]. He conservatively assumed that the web-flange juncture could be idealized as a simple support and treated the web as a rectangular plate that was simply supported on all four sides.

Fig. 2 illustrates the assumptions of Basler’s model. The tension field with initial applied load V_1 ($V_1 > V_{cr}$), initial inclination θ_1 , and initial width s_1 will continue to increase in width up until s_3 , which is when the ultimate shear buckling load has been reached. As the tension field increases in width from s_1 to s_3 , in order for the flexible flanges assumption to be maintained, the inclination of the tension field must change from θ_1 to θ_3 such that the vertical transverse stiffeners anchor the tension field.

The Basler–Thürlimann solution presented in Eq. (5) is an amended form of the original published solution based on the work of several authors such as Gaylord, Fujii, and Selberg [8,21–24]. The modifications to the original equations were made so that the true width of the tension field was considered, resulting in:

$$\tau_u = \tau_{cr} + \sigma_{yw} \left(1 - \frac{\tau_{cr}}{\tau_{yw}} \right) \left(\frac{\sin \theta_d}{2 + \cos \theta_d} \right) \quad (5)$$

where τ_{cr} is the value computed from Eq. (1), σ_{yw} is the web yield stress in tension, τ_{yw} is the web yield stress in shear, and θ_d is the angle of the panel diagonal. τ_{yw} is calculated as 0.6 σ_{yw} based on the *AISC Steel Construction Manual* [25]. Inelastic buckling is assumed to occur if τ_{cr} calculated from Eq. (1) is greater than 0.8 τ_{yw} ; in this case, τ_{cr} in Eq. (5) is replaced with:

$$\tau_{cr,i} = \sqrt{0.8\tau_{cr}\tau_{yw}} \quad (6)$$

where τ_{cr} in Eq. (6) is calculated from Eq. (1).

Following the development of the Basler model, Porter et al. (1975) developed a more robust analytical model accounting for the contribution of the flexural capacity of the flanges to determine the postbuckling shear strength. Their model, known as the *Rockey or Cardiff model*, forms the basis of *British Standard 5400 (1982)* [16], and assumes that ultimate shear buckling strength occurs when plastic hinges form in the flanges, resulting in a collapse mechanism [8,26]. The Basler model is a specialized case of the Rocky model. By assuming that the flanges are too flexible to resist flexure, the Rocky model simplifies to the Basler solution [26].

3. Validation study: finite element models

Finite element (FE) models will be used to evaluate the adequacy of Eq. (5) at elevated temperatures, which are validated based on previous experiments [9,10,20,27]. This section gives details of the FE models,

which are used in the validation and parametric studies to evaluate the adequacy of Eq. (5). The results of the validation study are presented in Section 4.

3.1. Prototypes

Researchers from Nanyang Technological University published data in 2007 from physical experiments designed to test the web shear buckling capacity of steel plate girders at elevated temperatures [10,9]. The plate girders they tested had web plates with depths ranging from 139 mm to 305 mm, thicknesses of 1.5 mm to 6.1 mm, and web slenderness ratios of 22.8 to 203.3. These test specimens had web depths that were significantly smaller than bridge plate girders, which typically have depths in excess of 1 m [12].

Of the five test girder (TG) specimens that were tested, TG3 and TG4 were selected for the FE model validation due to their size and high slenderness ratios. TG5 was not selected due to its very thin, 1.5 mm-thick web. A web plate with a 1.5 mm thickness is substantially thinner than the smallest allowable fillet weld size in the *AISC Steel Construction Manual* [25]. TG3 and TG4 also used web plates that are thinner than the smallest allowable fillet weld size, but they were used for the model validation because their webs are the thickest of the plate girders tested in [10]. TG1 and TG2 were neglected because they had small slenderness ratios (less than 23) and were not susceptible to web shear buckling.

The dimensions of the TG3 and TG4 test specimens are presented in Table 1, where a is the span, D is the depth (clear distance between flanges), t_w is the web thickness, b_f is the width of the flange, and t_f is the flange thickness. E_w and E_f refer to the ambient temperature Young’s modulus values of the web and flange, respectively, while σ_{yw} and σ_{yf} refer to the ambient temperature yield strength of the web and flange, respectively.

The TG3 and TG4 specimens had unusually small dimensions due to the test furnace setup. To ensure confidence in the FE methods employed in this paper, additional model validations were conducted at ambient temperature with two test girders from experiments conducted at Lehigh University in the early 1960s by Basler et al. [20,27]. The two girders selected for our model validation were G6 and G7 since the dimensions (see Table 1) of these test specimens were readily available. The dimensions reported in Table 1 were converted from US customary; the D/t_w values were directly taken from the published report [20].

For TG3, experimental data for the ultimate shear buckling load, V_u , was collected at 20 °C, 400 °C, 565 °C, and 690 °C (approximated as 700 °C in the FE model). For TG4, experimental data was collected at 20 °C, 400 °C, 550 °C, and 700 °C. At 550 °C, the authors in [10] noted that there was an error with the experimental setup, thus experimental results at this temperature were not compared with the TG4 FE model. For G6 and G7, V_u data was only collected at 20 °C.

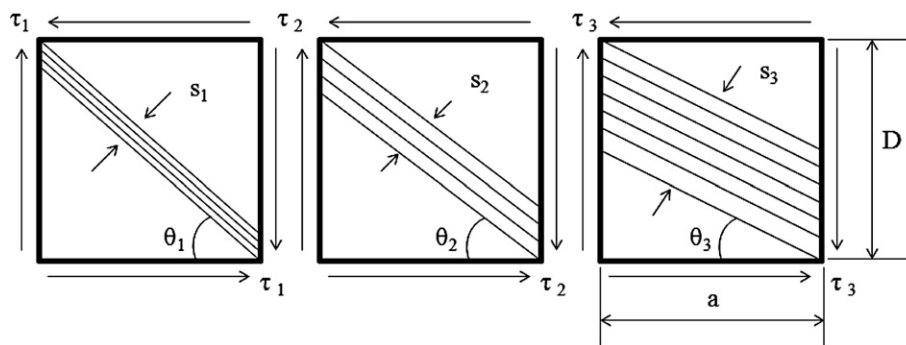


Fig. 2. Tension field model as proposed by Basler [8,20]. θ_i and s_i ($i = 1, 2, 3$) are the angle and width of the tension field, respectively. All four edges are assumed to be simply supported. τ_i represents the applied pure shear loading. As τ_i increases from τ_1 ($\tau_1 > \tau_{cr}$) to τ_3 , s_1 increases to s_3 and the corresponding θ_i must decrease from θ_1 to θ_3 to allow the vertical component from tension field to be resisted entirely by the transverse stiffener.

Table 1
Dimensions and material properties for TG3 and TG4, based on [10].

	Web						Flange				
	a	D	t_w	a/D	D/t_w	E_w	σ_{yw}	b_f	t_f	E_f	σ_{yf}
	(m)	(m)	(m)			(GPa)	(MPa)	(mm)	(mm)	(GPa)	(MPa)
TG3	0.305	0.305	0.002	1	152.5	200	287.8	0.08	0.006	204	274.5
TG4	0.305	0.305	0.0027	1	112.9	200	232.8	0.08	0.006	204	277
G6	1.905	1.27	0.005	1.5	266.7	200	250	305	19	200	250
G7	1.27	1.27	0.005	1	266.7	200	250	305	19	200	250

3.2. Mesh and boundary conditions

Two FE models, “Flange” and “SS”, were studied. The *Flange* model explicitly considers the contribution of the flanges to the buckling strength and the *SS* model assumes simply supported boundary conditions for the top and bottom flanges. All of the FE models were meshed with S4 (doubly curved, general-purpose, finite membrane strains) shell elements [11]. A mesh convergence study was conducted using an eigenvalue extraction analysis at 20 °C. The mesh densities shown in Fig. 3 had less than 1% error compared to the value of τ_{cr} computed from Abaqus with the value obtained from Eq. (1). The percent error was calculated from:

$$\%error = \frac{|\tau_{cr}^{FE} - \tau_{cr}^{Eq.(1)}|}{|\tau_{cr}^{Eq.(1)}|} \times 100 \tag{7}$$

Fig. 3 also shows the boundary conditions used in both FE models. It will be shown later that the boundary conditions of Fig. 3 result in good correlation with τ_{cr} of Eq. (1). Also, these boundary conditions allow a state of pure shear to develop; when side ② is loaded in the y-direction, the magnitude of the principal stresses in the plate equals the magnitude of the applied shear stress. Previous researchers that have studied web shear buckling for a simply supported plate [16] proposed boundary conditions that differ from those presented in Fig. 3. These researchers constructed a FE model for a plate with $a/D = 1.0$. While their proposed boundary conditions performed well at $a/D = 1.0$, we found that these boundary conditions were not robust for span-to-depth ratios greater than 1.0. For example, results obtained from an eigenvalue extraction analysis for $a/D = 1.4, 2.0,$ and 3.0 show that τ_{cr} values from the FE analyses are larger than those calculated using Eq. (1) if boundary conditions based on [16] were used.

3.3. Material model

The Eurocode material model [28], which specifies temperature-dependent reduction factors for the yield strength (σ_y) and Young’s

modulus (E), was assumed for the FE models. The authors in [10] assumed an elastic–perfectly plastic material model in their FE studies (also using Eurocode); therefore, the Eurocode reduction factor for the proportional limit stress, σ_p , was not included in their FE models. Using a “fully nonlinear” material model accounts for the development of nonlinear behavior between σ_p and σ_y at elevated temperatures (i.e., σ_p^T and σ_y^T , where the superscript “T” refers to elevated temperature values). This current study, therefore, examines the effect of neglecting this nonlinear range that develops at σ_p^T by comparing the results of FE models assuming elastic–perfectly plastic material properties to those with fully nonlinear material properties.

Fig. 4(a) shows plots of the Eurocode reduction factors for yield and proportional stress, $k_{y,T}$ and $k_{p,T}$, respectively, as a function of temperature. For $T \leq 100$ °C, $k_{y,T}$ and $k_{p,T}$ are both 1.0, thereby exhibiting elastic–perfectly plastic behavior in this range of temperatures. As the temperatures increase above 100 °C, $k_{p,T}$ becomes less than 1.0; for all $T \geq 100$ °C, $k_{p,T}$ continues to be smaller than $k_{y,T}$, meaning that a nonlinear behavior exists before the yield strain is reached.

The fully nonlinear material model is represented by the stress–strain curves shown in Fig. 4(b). Strain hardening is allowed by the Eurocode up to 400 °C [28] and is shown in Fig. 4(b) for 20 °C. Previous studies, however, have shown that allowing strain hardening does not significantly contribute to the mechanical behavior at elevated temperatures [29]. The yield stress, σ_y^T , is assumed to be reached at a yield strain of 0.02. For the remainder of this paper, whenever σ_y^T is used (or, similarly, σ_{yw}^T for the elevated temperature value of the web yield stress), this value is based on the Eurocode assumption of yield strain equal to 0.02.

3.4. Geometric imperfection

Buckling is a stability problem in which a bifurcation exists in the load–displacement curve, which exists because the initial defined geometry of the web plate is “perfect,” i.e. the plate is modeled as perfectly flat. Since a postbuckling analysis requires advancing the numerical solution beyond the bifurcation point in order for the ultimate shear buckling strength to be determined, the original perfect geometry of the web plate is perturbed with a small displacement field. A small scale of the

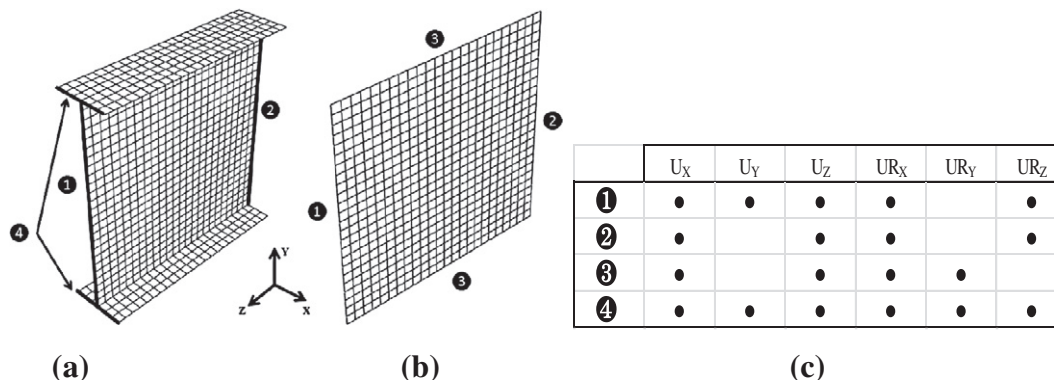


Fig. 3. Mesh and boundary conditions for the FE models: (a) *Flange* mesh; (b) *SS* mesh; (c) boundary conditions for the models where a “●” indicates a restrained degree of freedom.

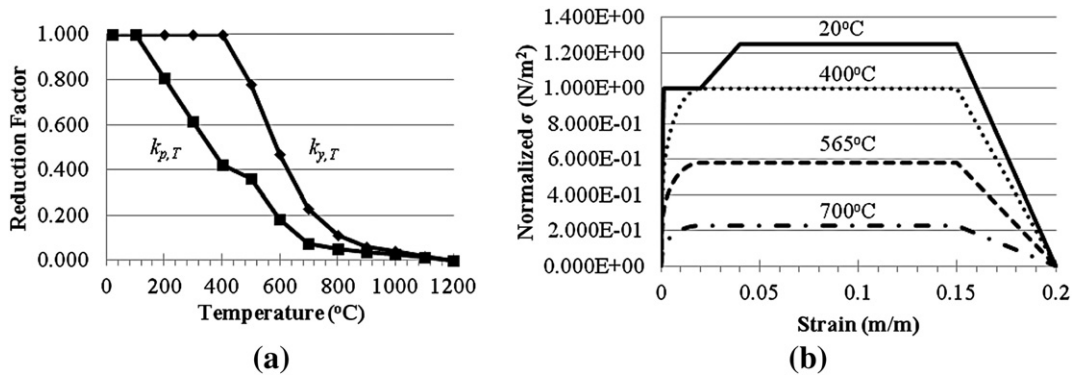


Fig. 4. Plots of (a) $k_{y,T}$ and $k_{p,T}$ versus temperature based on [28], and (b) stress–strain curves at 20 °C, 400 °C, 565 °C, and 700 °C for TG3 and TG4, where the stress is normalized by σ_y at ambient temperature, for the “fully nonlinear” material properties based on the Eurocode [28].

buckling mode shape typically associated with the lowest eigenvalue is used to create an imperfection in the original geometry, thus smoothing the load–displacement response of the structure and allowing the numerical solver to advance beyond the bifurcation [11]. Reference is made in the literature to the possibility of using a linear superposition of multiple buckling mode shapes to develop an appropriate initial imperfection [11]. This becomes important when the eigenvalues are closely spaced together; for the FE models studied in this paper, this is not the situation.

The imperfection magnitude in the FE models was generated by multiplying the lowest positive eigenmode shape (that has a maximum displacement of 1.0) by a scale factor. Previous work has suggested using a scale factor of $0.001 \cdot t_w$, where t_w is the web thickness, which proved sufficient for axial compression in plates exposed to fire [30]. For the current study, a scale factor of $D/10,000$ was used since it was found to be acceptable for advancing the nonlinear solver for the pure shear loading case considered in this study. This scale factor is consistent with previous work that has also studied the web shear buckling mechanism [16]. These previous researchers also investigated large scale factors up to $D/100$ and found that using a scale factor this large caused the nonlinear postbuckling analysis to predict a lower ultimate shear buckling strength and higher lateral displacements in the web plate.

4. Validation study: results

The FE model defined in Section 3 is used to predict both V_{cr} and V_u , both of which are then compared to the experimental results of TG3, TG4, G6, and G7. V_{cr} is calculated based on an eigenvalue extraction analysis. V_u is determined by the maximum value of the load–displacement curve as described in detail in Section 5.

4.1. Using elastic–perfectly plastic material properties

Table 2 compares the buckling values computed using the FE models with elastic–perfectly plastic material properties with the experimental values published in [10]. Results for both the SS and Flange models are shown. The table shows that the Flange FE model V_{cr} values are larger than those of the SS FE models, indicating that the flange has some stiffening effect on the FE V_{cr} results. The effect of the flange on the FE V_u results, however, is significantly less and essentially negligible. These results indicate that in the postbuckling range (from elastic critical to ultimate buckling), the flange-to-web juncture for these particular models possesses little rotational stiffness, behaving more like a simple support.

For both TG3 and TG4, the experimental V_{cr} values correlated better with the SS models compared to the Flange models, except that at 20 °C and 700 °C for TG3, the Flange FE model had better correlation. It is possible that the weld connection of the very thin webs to the flange may have contributed to the observed simply supported behavior during the experiments. The G6 and G7 SS specimens also had good agreement between the FE and experimental V_{cr} values.

For the comparison of V_u , Table 2 shows that again the V_u experimental values agree more closely to the SS FE model values than the Flange model. At 565 °C for TG3, and at 400 °C and 700 °C for TG4, both the Flange and SS FE models predict a substantially larger V_u value compared with the reported experimental value. These observations can be clearly seen from the performance ratios that compare the V_u values determined from the Flange and SS FE models with the Experiment value (Flange/Exp and SS/Exp). The G6 and G7 specimens, which were only tested at 20 °C, have V_u FE values that are in good agreement with the experimental data.

We hypothesized that these large discrepancies in performance ratios may be due to the simplified elastic–perfectly plastic material

Table 2

Comparison of FE V_{cr} (kN) and V_u (kN) values from the current study with the experimental results published in [10] for TG3 and TG4 assuming elastic–perfectly plastic material properties.

Model	T (°C)	V_{cr} (kN)			V_u (kN)			V_u performance ratios	
		FE model		Experiment	FE model		Experiment	Flange/Exp	SS/Exp
		Flange	SS		Flange	SS			
TG3	20	56.69	44.85	53.35	83.06	81.87	79.85	1.04	1.03
	400	39.69	31.40	30.08	79.26	77.57	67.63	1.17	1.15
	565	23.36	18.48	19.87	45.95	44.99	34.34	1.34	1.31
	700	7.37	5.83	7.05	17.68	17.18	17.15	1.03	1.00
TG4	20	139.5	110.6	101.4	106.3	102.9	111.8	0.95	0.92
	400	97.61	77.4	58.9	99.1	96.5	77.1	1.29	1.25
	700	18.13	14.4	10.59	21.9	21.4	15.94	1.27	1.34
G6	20	181.53	127.16	121.9	552.8	538.0	516	1.07	1.04
G7	20	217.46	167.28	167.3	672.8	643.2	645	1.04	1.00

Table 3
Comparison of FE V_u (kN) values from the current study with experimental results published in [10] for TG3 and TG4 assuming a fully nonlinear material model.

Model	T (°C)	V_u (kN)		Experiment	Performance ratios	
		FE model			Flange/Exp	SS/Exp
		Flange	SS			
TG3	20	83.06	82.37	79.85	1.04	1.03
	400	83.14	69.40	67.63	1.23	1.03
	565	48.15	40.16	34.34	1.40	1.17
	700	18.83	15.75	17.15	1.10	0.92
TG4	20	106.30	102.95	111.8	0.95	0.92
	400	101.63	82.92	77.1	1.32	1.08
	700	22.93	18.87	15.94	1.44	1.18
G6	20	552.8	538.0	516	1.07	1.04
G7	20	672.8	643.2	645	1.04	1.00

model assumed in the FE analyses. As noted earlier, this material model ignores large nonlinear behavior that develops well in advance of the yield strain as shown in Fig. 4(b). Therefore, the current study was repeated using the fully nonlinear material properties of steel as discussed next.

4.2. Using fully nonlinear material properties

Table 3 compares the FE and experimental values of V_u where the fully nonlinear material model was used in the FE analyses. From Table 3, it can be seen from the performance ratios that the experimental V_u values correlated better with the SS FE models than the Flange FE models. Further, comparison of Tables 2 and 3 shows that the FE models with fully nonlinear material properties (Table 3) have performance ratios closer to 1.0 — especially the SS FE models. The results for G6 and G7 are the same as those reported in Table 2 because nonlinear elastic behavior does not occur in the Eurocode model at 20 °C. All FE V_u results are in good agreement with their published experimental values at 20 °C, suggesting that the FE methods used in this paper are validated at ambient temperature.

4.3. Effect of uncertainties in elevated temperature steel material properties

The last column of Table 3 shows that the FE models that assume simple supports typically come within 8% of the experimental V_u . Exceptions are TG3 at 565 °C and TG4 at 700 °C, which yield results that are 17% and 18% larger than the experiments, respectively. One such reason for these discrepancies is the large uncertainty inherent in the material

properties of steel at elevated temperatures. This section examines the effects of steel material property uncertainties at elevated temperatures on the value of τ_u .

Previous work has been done to develop a probabilistic, performance-based framework for the evaluation of steel members in buildings subjected to fire [31]. As part of this framework, probabilistic models of steel material properties were developed to account for observed variations in these material properties at ambient and elevated temperatures [31,32]. More specifically, probabilistic equations for the E and σ_y reduction factors as a function of temperature ($k_{y,T_probabilistic}$ and $k_{E,T_probabilistic}$, respectively) were proposed:

$$k_{y,T_probabilistic} = \exp \left[\ln(k_{y,T}) - 0.0421 + 0.1464 \times \varepsilon \right] \tag{8}$$

$$k_{E,T_probabilistic} = 1.08 \times \frac{\exp(2.93 - 3.2 \times 10^{-3} - 3.2 \times 10^{-6}T^2 + 0.317\varepsilon)}{\exp(2.93 - 3.2 \times 10^{-3} - 3.2 \times 10^{-6}T^2 + 0.317\varepsilon + 1)} \tag{9}$$

In both equations, T refers to the temperature in Celsius; $k_{y,T}$ refers to the deterministic, temperature-dependent σ_y reduction factor from [28]; and ε is a standard normal variable with mean of 0 and standard deviation of 1. The value of ε was randomly selected for each iteration of the Monte Carlo simulation based on the prescribed constraints. While Eq. (8) is based on the Eurocode [28], it corrects the deterministic $k_{y,T}$ to fit measured data. Therefore, if $k_{y,T_probabilistic}$ were derived based on NIST’s deterministic model for $k_{y,T}$ [32], the new Eq. (8) would have yielded similar results since the same data is used to correct the deterministic model.

Fig. 5 shows the results from the Monte Carlo simulation based on specimens TG3 and TG4. The deterministic (x -axis) values are based on Eq. (5) using Eurocode material properties [28]. The Monte Carlo (y -axis) τ_u values are also based on Eq. (5), but use Eqs. (8) and (9) for the material properties. These values are based on a four-sided simply supported web plate since Eq. (5) is based on the assumption that the flange–web juncture is idealized as a simple support.

Fig. 5 also shows how the experimental and FE results compare with their respective probability density functions developed from the Monte Carlo simulations. It is seen that both the FE τ_u values (based on the SS model with fully nonlinear material properties) and experimental τ_u values are within the stochastic range of τ_u values.

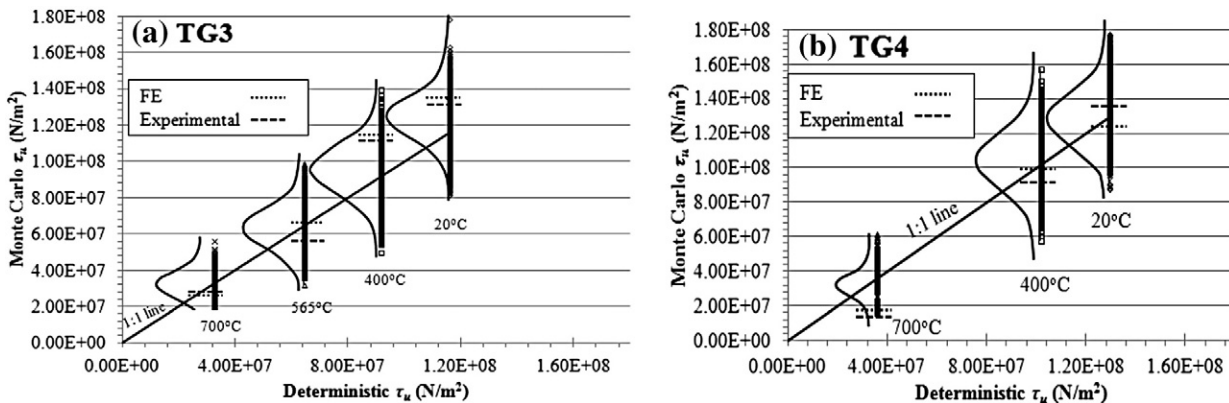


Fig. 5. Monte Carlo τ_u values (y -axis) compared to deterministic τ_u values, both calculated from Eq. (5): (a) TG3 and (b) TG4. Probability distribution functions are drawn based on the Monte Carlo simulation results.

4.4. Conclusions of validation study

Three key conclusions are drawn from the validation study presented in this section and form the basis for the FE model to be used in the studies to follow:

- (1) At elevated temperatures, it is best to use the fully nonlinear material model and not simplify the analysis with elastic–perfectly plastic properties. In the range of elevated temperatures expected in a fire, steel becomes nonlinear before the Eurocode defined yield strain ($= 0.02$) is reached. With plate buckling limit states in particular, including this early nonlinear behavior is important. This conclusion was also observed in axial buckling studies of steel plates at elevated temperature [30]. If elastic–perfectly plastic properties are used, a careful evaluation of the definition of “yield stress” needs to be made. The parametric studies to follow will therefore use the fully nonlinear material model.
- (2) For the experiments used in this validation study, the FE models that used simply supported boundary conditions (SS models) correlated better to the test results than the models that explicitly modeled the flanges (Flange models). The reason that the SS FE models correlated better to test results could be related to the web–flange weld connection of these particular specimens. At elevated temperatures, this connection may have had little or no rotational restraint. In the parametric studies to follow, simple supports will be used to represent the flanges. While the authors recognize that in some cases the flange–web connection may show some rotational restraint, to assume that it does not is reasonably conservative.
- (3) The results of the Monte Carlo simulation study have shown that considering the uncertainties of yield stress and modulus of elasticity of steel at elevated temperatures results in a relatively large range of possible τ_{cr} values. This effect of material uncertainty should be considered qualitatively, if not quantitatively, in evaluations of plate buckling at elevated temperature.

5. Effects of a/D and Temperature on plate buckling

With the model that was discussed in Section 3, and validated as shown in Section 4, a study of plate buckling is discussed in this section with the parameters being a/D ratio and temperature. This study forms the basis for evaluating the adequacy of Eq. (5) at elevated temperatures.

5.1. FE models

FE models of simply supported rectangular web plates were developed based on the physical parameters for a typical 90 foot (27.43 m) span of a steel plate girder bridge [12]. The web depth, D , and web thickness, t_w , were specified as 1.47 m and 0.011 m, respectively, and the corresponding slenderness ratio (D/t_w) was 134 [12]. The span-to-depth ratios (a/D) varied in the study as follows: 1.4, 2.0, and 3.0. The span, a , represents the spacing of transverse stiffeners in a bridge girder. The a/D value of 1.4 corresponds with the recommended transverse

stiffener arrangement [12], while the values of 2.0 and 3.0 were selected to study the effect of increasing the span-to-depth ratio. The accuracy of Eq. (5) is known to decrease significantly when $a/D \geq 3.0$ [33], thus our study did not include larger a/D values. A sketch of the three FE models and their geometry is shown in Fig. 6.

The boundary conditions are the same as those validated in Section 3: simple supports on all edges as represented in Fig. 3. Fully nonlinear material properties of steel were used as demonstrated in Fig. 4. A36 steel was selected based on a previous case study [34,35]. At ambient temperature, σ_{yw} and E were taken as 250 MPa and 2×10^{11} N/m², respectively, and $\nu = 0.3$. The elevated temperature material properties for E and σ_{yw} were calculated using Eurocode reduction factors [28]. The initial imperfection was modeled as explained in Section 3.

Nonlinear postbuckling analyses are a computationally expensive means of determining the optimized mesh [30], while the eigenvalue extraction analysis is fast and allows mesh convergence to be checked against τ_{cr} values calculated using Eq. (1). Therefore, mesh convergence studies were conducted on all three FE models using the results from an eigenvalue extraction analysis at 20 °C with S4 shell elements [11]. The mesh chosen for the parametric study was selected based on percent error (Eq. (7)) coupled with required computational effort (represented by the number of elements). The selected meshes have 609, 1711, and 1850 elements corresponding to a/D of 1.4, 2.0, and 3.0, respectively, as shown in Fig. 6. Percent errors equal 2.4, 4.1, and 2.0 corresponding to a/D values of 1.4, 2.0, and 3.0, respectively.

5.2. Elastic critical shear buckling stress, τ_{cr} , at elevated temperatures

The theoretical (computed from Eq. (1)) and FE τ_{cr} values were calculated at 20 °C, 100 °C, and 100 °C increments up to 1100 °C (at 1200 °C, the Eurocode assumes the values of E and σ_{yw} are zero). All analyses were conducted at steady state, thus the FE model was considered uniformly heated. This steady state analysis is consistent with previous experimental work that tested web shear buckling at elevated temperatures [10,9].

A comparison of the FE results with those computed from Eq. (1) shows that for all three FE models, the numerical and closed-form solution τ_{cr} values are in good agreement. Ratios of theoretical τ_{cr} values to FE τ_{cr} values equal 0.99, 0.95, and 0.97 for $a/D = 1.4, 2.0,$ and $3.0,$ respectively, for the full temperature range. These results indicate that the existing elastic theory is applicable at the higher temperatures of interest, which is not surprising since the only variable in Eq. (1) that varies with temperature is Young's modulus, E , and both the FE analyses and Eq. (1) use the Eurocode [28] reduction factors to compute E at elevated temperatures.

Fig. 7 shows the displacement fields from an eigenvalue extraction analysis conducted at 20 °C for the simply supported web plates analyzed. Due to symmetry, the two lowest eigenvalues that are extracted will be negative inverses of each other, which physically implies that the web plate will buckle at the same load regardless of the direction of the shear load vectors shown in Fig. 7. To create the initial geometric imperfection for the nonlinear postbuckling analysis, the displacement

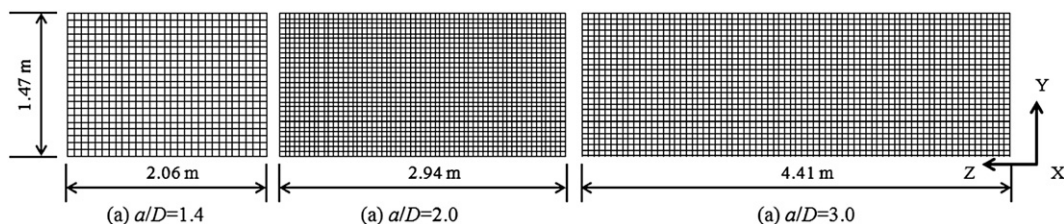


Fig. 6. Geometry and mesh used in the parametric study of plate girder webs.

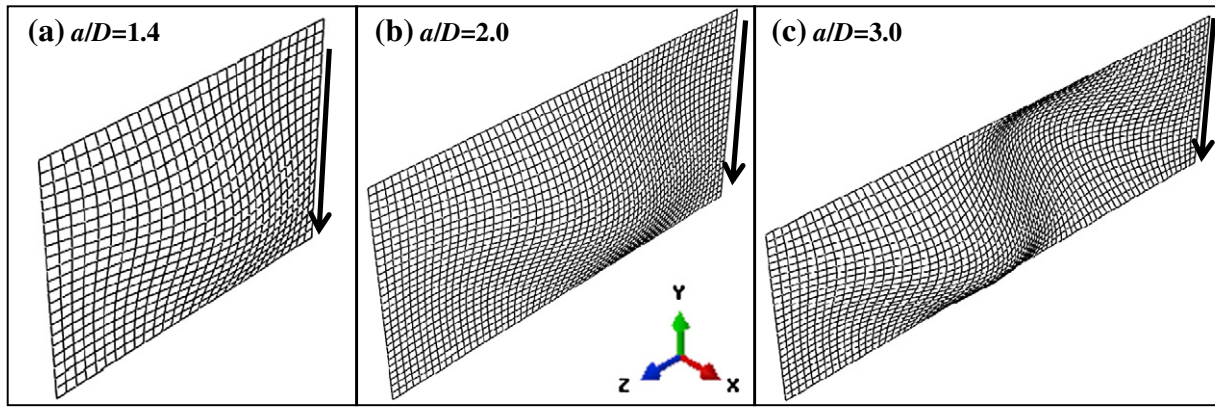


Fig. 7. Displacement field results from an eigenvalue extraction analysis at 20 °C. The arrows represent the direction of the shear load vectors.

fields shown in Fig. 7 were multiplied by the $D/10,000$ scale factor as discussed in Section 3.

5.3. Ultimate shear buckling load, V_u , at elevated temperatures

V_u was determined by examining the load–displacement plots. For illustration, Fig. 8 plots the load–displacement curves of (1) the vertical (y) displacement measured at the bottom right-hand corner of the web plate (Δ_{corner}) and (2) the out-of-plane (x) displacement measured approximately at the center of the diagonal buckle (δ_{center}) for a web plate with $a/D = 2.0$ and a temperature of 20 °C. Fig. 8(a) plots load–displacement of the full analysis run (meaning the nonlinear solver runs until it no longer converges or completes the number of analysis steps input by the user). Determining the sufficient number of analysis steps to capture V_u was done in a heuristic manner.

Fig. 8(b) zooms in on Fig. 8(a) on the smaller areas of displacement where the first change in slope is observed in the load versus Δ_{corner} plot. The first change in stiffness of this load–displacement curve (at approximately 1.08×10^6 N) corresponds with V_{cr} . V_u was determined as the point where the load–displacement curve becomes horizontal or reverses slope. Fig. 8(a) shows that both the center and corner nodes mark V_u at the same value. Fig. 8(b) focuses on load versus Δ_{corner} because V_{cr} may be easily read from this plot. V_{cr} is more difficult to interpret from the load versus δ_{ctr} plot because the first change in stiffness is sensitive to the location where δ_{ctr} is measured on the diagonal tension field.

Table 4 shows the results of the FE analysis at the postbuckling stage. Since the length of each plate, a , varied, Δ_{corner}/a is also shown for comparison of the corner displacement of the three plates and essentially represents the plate slope at failure. The slope at failure is typically 0.002 for temperatures less than 400 °C and 0.001 for temperatures greater than 800 °C. For temperatures from 400 °C to 800 °C the slope, as well as δ_{ctr} , are much larger compared to the other temperature

ranges. This range coincides with temperatures where the values of $k_{y,T}/k_{p,T}$ (see Fig. 4(a)) are larger than at other temperatures. In this range, the steel material loses stiffness well before the yield strain. Therefore, larger displacements occur before V_u is reached.

Fig. 9 shows images of plate deformations when V_u is reached for $a/D = 1.4, 2.0,$ and 3.0 at 200 °C (lower temperature range), 500 °C (mid-temperature range), and 800 °C (upper temperature range), respectively. Notice that the diagonal buckles in Fig. 9(b) and (c) are quite pronounced, while the diagonal buckle in Fig. 9(a) is present, albeit less distinct.

5.4. Summary of a/D study

The FE analyses are capable of predicting τ_{cr} well, compared to the theoretical solution of Eq. (1), for all a/D ratios and temperatures. At the postbuckling stage, it is observed that V_u decreases with increasing temperature in correlation with the elevated material properties. Some trends for V_u are not the same for all temperatures, however. For example, in the mid-range (400 °C to 800 °C) where $k_{p,T}/k_{y,T}$ values are the largest, the plate deformation at V_u is larger than at other temperatures. This relationship between V_u and the material is examined next.

6. Evaluation of Basler–Thürlimann’s theoretical equation at elevated temperatures

Using the results of the a/D study, the Basler–Thürlimann theoretical equation for predicting the τ_u value of plates (Eq. (5)) is evaluated at elevated temperatures. This is done by replacing σ_{yw} with the stress at the ultimate condition, σ_{yw}^T . Hence, τ_{yw} in Eq. (5) is then equal to $0.6\sigma_{yw}^T$.

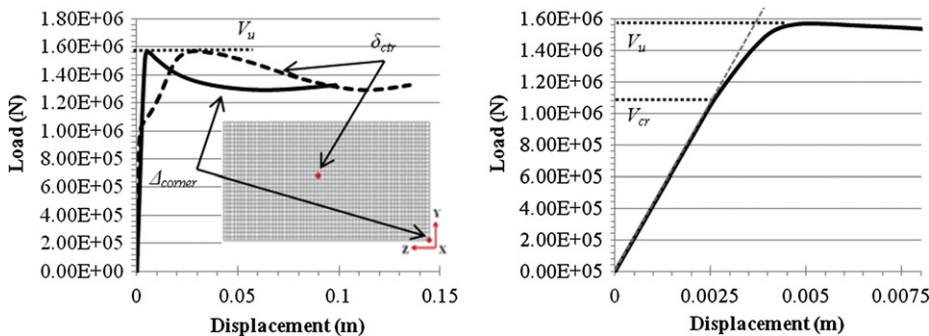


Fig. 8. Load–displacement curves for $a/D = 2.0$ at a temperature of 20 °C: (a) full analysis, and (b) zoom-in of Fig. 8(a) for Δ_{corner} .

Table 4
Postbuckling results.

T (°C)	a/D = 1.4				a/D = 2.0				a/D = 3.0			
	V_u	δ_{center}	Δ_{corner}	Δ_{corner}/a	V_u	δ_{center}	Δ_{corner}	Δ_{corner}/a	V_u	δ_{center}	Δ_{corner}	Δ_{corner}/a
	(kN)	(m)	(m)		(kN)	(m)	(m)		(kN)	(m)	(m)	
20	1787	0.026	0.004	0.002	1574	0.029	0.005	0.002	1515	0.023	0.009	0.002
100	1787	0.026	0.004	0.002	1574	0.029	0.005	0.002	1515	0.023	0.009	0.002
200	1544	0.033	0.006	0.003	1364	0.030	0.005	0.002	1314	0.024	0.009	0.002
300	1829	0.159	0.189	0.092	1486	0.214	0.237	0.081	1108	0.024	0.009	0.002
400	1486	0.115	0.095	0.046	1251	0.185	0.178	0.061	1107	0.093	0.127	0.029
500	1164	0.114	0.092	0.045	1014	0.225	0.251	0.085	872	0.021	0.007	0.002
600	697	0.117	0.098	0.048	605	0.224	0.251	0.085	517	0.027	0.010	0.002
700	339	0.120	0.104	0.050	299	0.239	0.287	0.098	250	0.112	0.191	0.043
800	165	0.113	0.091	0.044	146	0.017	0.003	0.001	123	0.018	0.006	0.001
900	82	0.019	0.003	0.001	78	0.015	0.003	0.001	74	0.016	0.005	0.001
1000	55	0.025	0.004	0.002	52	0.015	0.003	0.001	49	0.017	0.005	0.001
1100	27	0.013	0.002	0.001	26	0.015	0.003	0.001	25	0.016	0.005	0.001

6.1. Replacing σ_{yw} with $k_{y,T}\sigma_{yw}$

τ_u versus temperature for FE models is compared to predictions of Eq. (5) with σ_{yw} replaced with $\sigma_{yw}^T = k_{y,T}\sigma_{yw}$ (this solution is referred to as BT- k_y) in Figs. 10(a), (b), and (c) for $a/D = 1.4, 2.0,$ and $3.0,$ respectively. While both the FE and BT- k_y solutions follow the same general trend, there are some differences to be noted.

Fig. 10(d) plots the BT- k_y /FE ratio to clearly show the difference between the two solutions. It shows that Eq. (5) appears to underestimate τ_u for all temperatures less than about 800 °C. This underestimation generally is less than 20%.

Observing Fig. 10(a), (b), and (c), a ‘wave’ in the τ_u -temperature plot is seen between 200 °C and 400 °C for the FE results, but this wave is not present in the BT- k_y plots. It will be shown later that this wave is due to σ_{yw}^T values at 200 °C and 300 °C that do not equal $k_{y,T}\sigma_{yw}$ (in the FE solutions) when V_u is reached.

Selamet and Garlock [30] studied steel plate buckling under axial loads at elevated temperature. They observed that the postbuckling stress at the edge of the plate, $\sigma_{e,T}$, is significantly smaller than the yield stress at 0.02 strain ($\sigma_{y,2\%}$) and the edge strains are significantly lower than 0.02. Predictive equations based on an edge stress equal to $\sigma_{e,T} = k_{0.2,T}\sigma_{y,2\%}$, or $\sigma_{e,T} = \sqrt{k_{y,T}k_{p,T}}\sigma_{y,2\%}$ (rather than $\sigma_{y,2\%}$) were found to offer a better correlation in plate postbuckling strength at elevated temperature when compared to the FE results. $k_{0.2,T}$ is a temperature-dependent 0.2% offset yield strength reduction factor given in the Eurocode [28]. In light of previous research and observations from the current study, alternative substitutions for σ_{yw} in Eq. (5) are examined next.

6.2. Replacing σ_{yw} with $k_{p,T}\sigma_{yw}$

τ_u versus temperature for the FE models is compared to predictions of Eq. (5) with σ_{yw} replaced with $\sigma_{yw}^T = k_{p,T}\sigma_{yw}$ (this solution is referred to as BT- k_p) in Fig. 11 for $a/D = 1.4, 2.0,$ and $3.0.$ For all FE models from 20 °C up to and including 800 °C, the BT- k_p /FE values are less than 1.0 and more conservative than the BT- k_y /FE values from Section 6.1. From 900 °C up to and including 1100 °C, the BT- k_p solution comes close to the FE values except for $a/D = 1.4.$

6.3. Replacing σ_{yw} with $\sqrt{k_{y,T}k_{p,T}}\sigma_{yw}$

Based on the previous work by Selamet and Garlock [30], σ_{yw} in Eq. (5) was replaced with $\sigma_{yw}^T = \sqrt{k_{y,T}k_{p,T}}\sigma_{yw}$. This solution, BT- $\sqrt{(k_p k_y)}$, is compared with the FE τ_u values in Fig. 12 for $a/D = 1.4, 2.0,$ and $3.0.$ It is seen that the BT- $\sqrt{(k_p k_y)}$ solution comes closer to the FE solutions than the BT- k_p values for $T \leq 800$ °C, but for $T > 800$ °C the BT- k_p solution comes closer to the FE values.

6.4. Replacing σ_{yw} with maximum von Mises stress in the tension field

The analytical solution presented in Eq. (5) is based on the assumption that the maximum stress in the tension field at V_u is the yield strength of the web steel, σ_{yw} . This section replaces σ_{yw} with the stress observed in the FE analyses when V_u is recorded. For each of the FE models, the von Mises stresses (σ_{Mises}) were extracted at an element located within the center of the diagonal tension field (Fig. 13), which is the location where, theoretically, the stresses are largest.

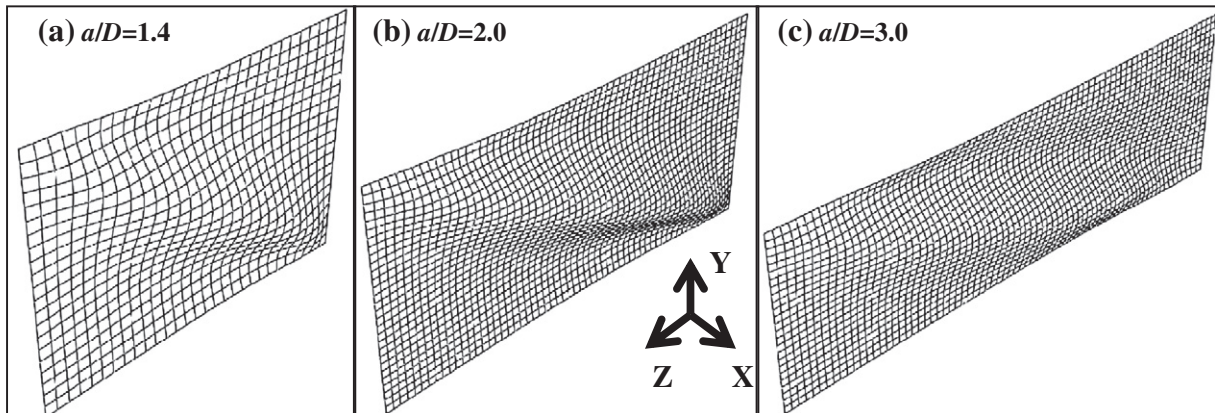


Fig. 9. Deformations when V_u is reached at 500 °C for $a/D =$ (a) 1.4, (b) 2.0, and (c) 3.0.

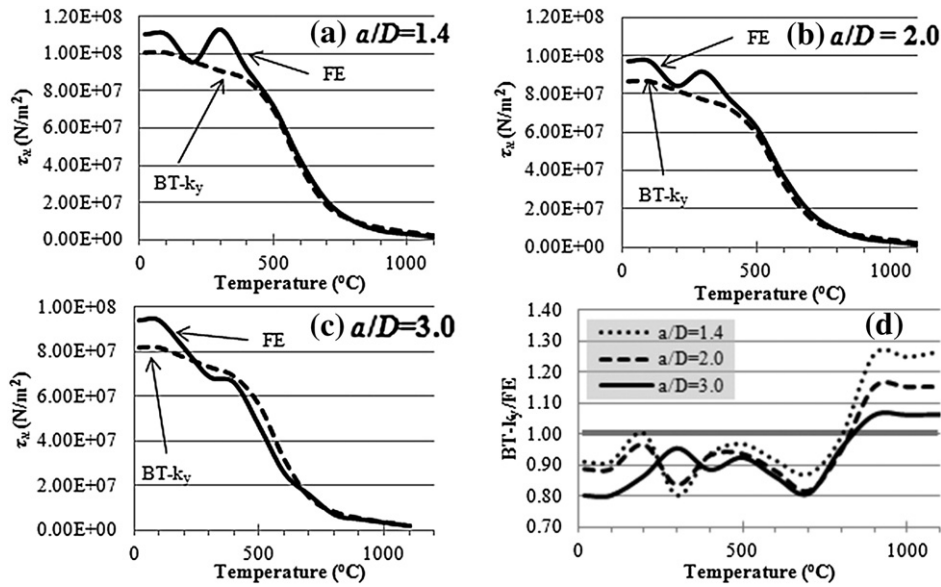


Fig. 10. Comparison of FE versus Eq. (5) predictions of τ_u with σ_{yw} replaced with $\sigma_{yw}^T = k_{y,T}\sigma_{yw}$ in Eq. (5) (BT- k_y). (a) $a/D = 1.4$, (b) $a/D = 2.0$, (c) $a/D = 3.0$, and (d) ratio of differences for all a/D studies and all temperatures.

Fig. 14 illustrates how σ_{Mises} at V_u was determined. The figure plots load–displacement curves from the $a/D = 1.4$ FE model at 200 °C, along with corresponding plots of σ_{Mises} versus number of increments up until V_u is reached. The horizontal dotted line labeled V_u in the load–displacement curves of Fig. 14(a) indicates the estimated V_u value for the FE models. The vertical dotted line in Fig. 14(b) indicates that the σ_{Mises} versus increment plot was truncated at the increment where V_u was read from the corresponding load–displacement curve.

SP:1 and SP:5 in Fig. 14(b) refer to section points 1 and 5. In Section 3.2, it was stated that S4 shell elements were used for the FE analysis in Abaqus [11]. Each shell element has 4 integration points, and each integration point has 5 section points through the thickness of the shell. When σ_{Mises} is extracted at each of the elements shown in Fig. 13, Abaqus displays the results at SP:1 and SP:5 for each integration point. To construct the plots shown in Fig. 14(b), the σ_{Mises} values corresponding to SP:1 and SP:5 for each of the four integration points are averaged. When SP:1 and SP:5 are not equal, it is an indication of bending in the plate (in this case due to buckling deformation).

Table 5 documents the temperature-dependent $k_{y,T}\sigma_{yw}$ values for each FE model and the corresponding σ_{Mises} values recorded from the elements highlighted in Fig. 13 when V_u is reached. Only $\sigma_{yw}^T = k_{y,T}\sigma_{yw}$ is compared in this section since it had the best correlation with the FE results as shown previously (see Fig. 10). For most temperatures, the

σ_{Mises} values recorded up to V_u match exactly the σ_{yw}^T value. At 200 °C, 300 °C, 900 °C, and 1100 °C, it was observed that the maximum σ_{Mises} value for the element in the middle of the diagonal tension field up to V_u was typically less than σ_{yw}^T . This implies that for some temperatures, the assumption in Eq. (5) that the steel in the diagonal tension field has reach σ_{yw}^T is not correct. Further, for $a/D = 1.4$ and 2.0 at 300 °C it is noted that σ_{Mises} is larger than σ_{yw}^T due to strain hardening of the material as allowed by the Eurocode [28].

Table 6 compares predictions of the BT solutions (Eq. (5)) with FE solutions through ratios, where BT- σ_{Mises} represents the value of τ_u predicted from Eq. (5) by replacing σ_{yw} in Eq. (5) with the maximum σ_{Mises} observed in the elements shown in Fig. 13 for the three FE models. For temperatures 900 °C and greater, BT- σ_{Mises}/FE is closer to 1.0 compared to BT- k_y/FE . These are the temperatures where σ_{Mises} is less than $k_{y,T}\sigma_{yw}$ as observed in Table 5. At 200 °C, using the maximum σ_{Mises} value resulted in a decreased correlation between Eq. (5) and the FE models, but this change was not large.

6.5. Summary of Basler–Thürlimann (BT) equation study

It was found that substituting σ_{yw} with $\sigma_{yw}^T = k_{y,T}\sigma_{yw}$ in the BT solution (Eq. (5)) yields results that are closest to the FE solution. Substituting $\sigma_{yw}^T = k_{p,T}\sigma_{yw}$ or $\sqrt{k_{y,T}k_{p,T}}\sigma_{yw}$ leads to more conservative solutions (where the BT solution values are much smaller than the FE solutions).

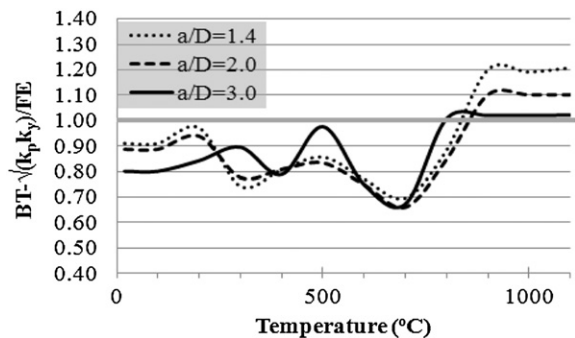
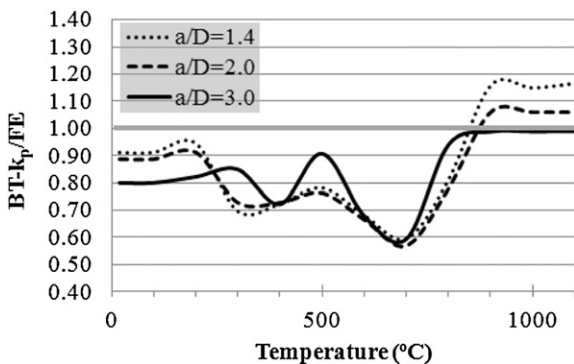


Fig. 11. Ratio of Eq. (5) versus FE predictions of τ_u with σ_{yw} replaced with $\sigma_{yw}^T = k_{p,T}\sigma_{yw}$ in Eq. (5) (BT- k_p).

Fig. 12. Ratio of Eq. (5) versus FE predictions of τ_u with σ_{yw} replaced with $\sigma_{yw}^T = \sqrt{(k_{p,T}k_{y,T})} \cdot \sigma_{yw}$ in Eq. (5) (BT- $\sqrt{(k_p k_y)}$).

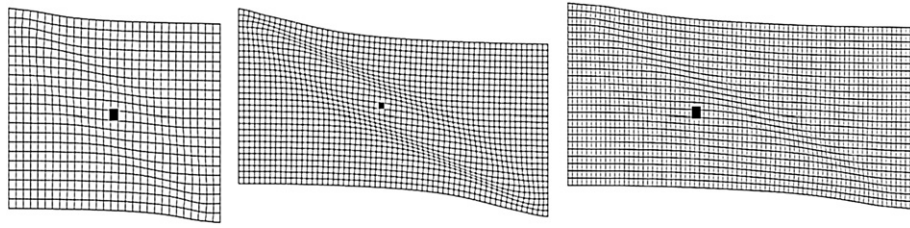


Fig. 13. Displacement fields at V_u at 700 °C for, from left to right, a/D of (a) 1.4, (b) 2.0, and (c) 3.0. The black square located approximately in the center of the buckled shape is also approximately at the center of the diagonal tension field and is the location where σ_{Mises} values were extracted.

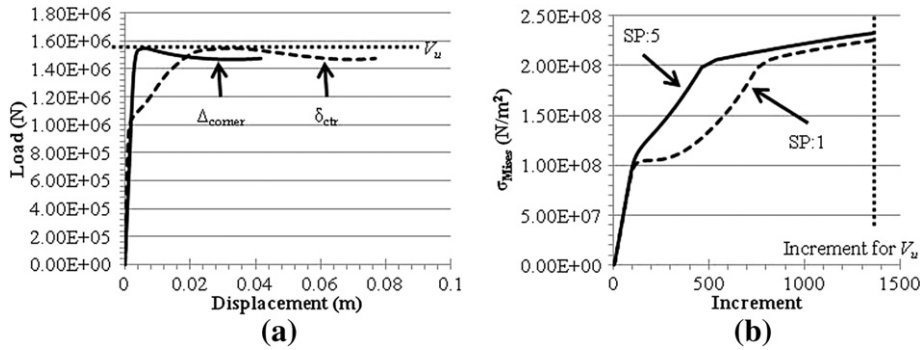


Fig. 14. (a) Load–displacement curve for $a/D = 1.4$ at 200 °C, and (b) corresponding σ_{Mises} plot up to V_u .

When the von Mises stresses (σ_{Mises}) were examined when V_u is reached, it is found that these stresses typically equal $k_y \tau \sigma_{yw}$ except at temperatures of 200 °C, 300 °C, and 900 °C to 1100 °C. In this range, V_u is reached at lower stresses (except for $a/D = 1.4$ and 2.0 at 300 °C where higher stresses are observed due to strain hardening).

Overall, it was found that the BT solution is sufficiently adequate at elevated temperatures provided that appropriate substitutions are made for σ_{yw} . For $20 \text{ °C} \leq T \leq 800 \text{ °C}$, substituting σ_{yw} with $\sigma_{yw}^T = k_y \tau \sigma_{yw}$ in the BT solution leads to results that agree well with the FE solution. For $T > 800 \text{ °C}$, the FE studies show that V_u is reached before $\sigma_{yw}^T = k_y \tau \sigma_{yw}$. In this range, best correlation is found when σ_{yw} is substituted with $k_{p,T} \sigma_{yw}$.

7. Summary and conclusions

The primary goal of this current study was to evaluate the Basler–Thürlimann (BT) equation (presented in Eq. (5)) at elevated temperatures by comparing ultimate shear buckling stress (τ_u) values predicted from this equation with those from finite element (FE) analyses. This

analytical solution had originally been developed at ambient temperature assuming elastic–perfectly plastic material properties. The FE investigations carried out in this paper characterized the postbuckling shear strength of web plates assumed to be simply supported at uniform, elevated temperatures. Working with a simply supported plate allowed for a direct comparison of FE results with those from the BT solution.

The following points summarize the findings of this study:

- (1) At elevated temperatures, FE models should use the fully nonlinear material model and not simplify the analysis with elastic–perfectly plastic properties. In the range of elevated temperatures expected in a fire, steel becomes nonlinear before the “yield” strain is reached, where yield, as defined by the Eurocode for example, is the ultimate or maximum stress reached at a strain of 0.02. With plate buckling limit states in particular, including this early nonlinear behavior is important.
- (2) The Monte Carlo simulation study indicated that considering the uncertainties of yield stress and modulus of elasticity of steel at elevated temperatures results in a relatively large range of

Table 5 Temperature-dependent σ_{yw} values and corresponding σ_{Mises} values for $a/D = 1.4, 2.0,$ and 3.0.

T (°C)	σ_{yw} (N/m ²)	σ_{Mises} (N/m ²)		
		$a/D = 1.4$	$a/D = 2.0$	$a/D = 3.0$
20	2.50E + 08	2.50E + 08	2.50E + 08	2.50E + 08
100	2.50E + 08	2.50E + 08	2.50E + 08	2.50E + 08
200	2.50E + 08	2.32E + 08	2.20E + 08	2.22E + 08
300	2.50E + 08	3.13E + 08	3.13E + 08	1.94E + 08
400	2.50E + 08	2.50E + 08	2.50E + 08	2.50E + 08
500	1.95E + 08	1.95E + 08	1.95E + 08	1.95E + 08
600	1.18E + 08	1.18E + 08	1.18E + 08	1.18E + 08
700	5.75E + 07	5.75E + 07	5.75E + 07	5.75E + 07
800	2.75E + 07	2.75E + 07	2.75E + 07	2.75E + 07
900	1.50E + 07	1.15E + 07	1.06E + 07	1.10E + 07
1000	1.00E + 07	7.94E + 06	7.04E + 06	7.39E + 06
1100	5.00E + 06	3.58E + 06	3.52E + 06	3.67E + 06

Table 6 Comparison of BT- k_y /FE and BT- σ_{Mises} /FE for all three FE models.

T (°C)	$a/D = 1.4$		$a/D = 2.0$		$a/D = 3.0$	
	BT- k_y /FE	BT- σ_{Mises} /FE	BT- k_y /FE	BT- σ_{Mises} /FE	BT- k_y /FE	BT- σ_{Mises} /FE
20	0.91	0.91	0.89	0.89	0.80	0.80
100	0.91	0.91	0.89	0.89	0.80	0.80
200	1.00	0.98	0.97	0.93	0.86	0.84
300	0.80	0.87	0.84	0.90	0.95	0.89
400	0.94	0.94	0.93	0.93	0.88	0.88
500	0.97	0.97	0.94	0.94	0.92	0.92
600	0.92	0.92	0.88	0.88	0.86	0.86
700	0.87	0.87	0.82	0.82	0.80	0.80
800	0.99	0.99	0.95	0.95	0.95	0.95
900	1.26	1.19	1.15	1.08	1.06	1.01
1000	1.25	1.19	1.15	1.08	1.06	1.01
1100	1.27	1.19	1.15	1.08	1.06	1.01

possible τ_u values. This effect of material uncertainty should be considered qualitatively, if not quantitatively, in evaluations of plate buckling at elevated temperatures.

- (3) The FE analyses are capable of predicting elastic shear buckling stress (τ_{cr}) well, compared to the theoretical solution of Eq. (1), for the a/D ratios studied (1.4, 2.0, 3.0) and elevated temperatures ($20^\circ\text{C} \leq T \leq 1100^\circ\text{C}$).
- (4) At the postbuckling stage, it is observed that the ultimate shear buckling load, V_u , decreases with increasing temperature in correlation with the elevated material properties. Some trends for V_u are not the same for all temperatures, however. For example, in the mid-range (400°C to 800°C), where the ratio of proportional limit stress to yield stress values at elevated temperatures ($k_{p,T}/k_{y,T}$) is the largest, the plate deformation at V_u is larger than at other temperatures.
- (5) FE results indicate that at temperatures of 200°C , 300°C , and 900°C to 1100°C , V_u is reached at stresses lower than the yield (except for $a/D = 1.4$ and 2.0 at 300°C where higher stresses are observed due to strain hardening).
- (6) Overall, the BT solution adequately predicts V_u (and therefore τ_u) at elevated temperatures provided that appropriate substitutions are made for σ_{yw} at elevated temperatures. It is recommended that for $20^\circ\text{C} \leq T \leq 800^\circ\text{C}$, σ_{yw} be substituted with $k_{y,T}\sigma_{yw}$. For $T > 800^\circ\text{C}$, σ_{yw} be substituted with $k_{p,T}\sigma_{yw}$.

The models presented thus far have only used simply supported boundary conditions in lieu of the flanges and have assumed a uniform temperature distribution across the web. Future work will include the flanges and will study web shear buckling in the presence of a thermal gradient. Additionally, the interaction of the transverse stiffeners with the web at high temperatures will be investigated to develop a more robust understanding of the web shear buckling mechanism.

Acknowledgments

This research was made with Government support under and awarded by DoD, Air Force Office of Scientific Research, National Defense Science and Engineering Graduate (NDSEG) Fellowship, 32 CFR 168a, provided to Mr. Glassman. This research was also sponsored by the National Science Foundation (NSF) under grant CMMI-1068252. All opinions, findings, and conclusions expressed in this paper are of the authors and do not necessarily reflect the policies and views of the sponsors.

References

- [1] Garlock M, Payá-Zaforteza I, Kodur V, Gu L. Fire hazard in bridges: review, assessment, and repair strategies. *Eng Struct* 2011;35:89–98.
- [2] email correspondence Maria Garlock with Michael Davidson. Lexington, KY: University of Kentucky; January 7, 2011.
- [3] Administration FH. Flexural capacity of fire-damaged prestressed concrete box beams (FHWA-HRT-07-024). FHWA; 2007.

- [4] Iqbal N, Salley MH, Weerakkody S. Fire dynamics tools (FDTs) quantitative fire hazard analysis methods for the U.S. Nuclear Regulatory Commission Fire Protection Inspection Program (NUREG-1805). Washington: GPO; 2004.
- [5] Kodur V, Aziz E, Dwaikat M. Evaluating fire resistance of steel girders in bridges. *J Bridg Eng* 2013;18(7):633–43.
- [6] Standard for road tunnels, bridges, and other limited access highways. National Fire Protection Association; 2008.
- [7] United States Department of Commerce. A survey of fuel loads in contemporary office buildings. MD: College Park; 1996.
- [8] Ziemian RD. Guide to stability design criteria for metal structures. 6th ed. Hoboken: John Wiley & Sons; 2010.
- [9] Vimonsatit V, Tan K-H, Ting S-K. Shear strength of plate girder web panel at elevated temperature. *J Constr Steel Res* 2007;63:1442–51.
- [10] Vimonsatit V, Tan K-H, Qian Z-H. Testing of plate girder web panel loaded in shear at elevated temperature. *J Struct Eng* 2007;133(6):815–24.
- [11] Dassault Systemes, "Abaqus 6.11ef Online Documentation," [Online]. [Accessed 2012].
- [12] FHWA, Federal Highway Administration. Standard plans for highway bridges. Structural Steel Superstructures, Volume II; 1982.
- [13] Timoshenko SP, Gere JM. Theory of elastic stability. Second Edition. New York: McGraw-Hill Book Company, Inc.; 1961.
- [14] Lee S, Davidson J, Yoo C. Shear buckling coefficients of plate girder web panels. *Comput Struct* 1996;59(5):789–95.
- [15] Lee SC, Yoo CH. Strength of plate girder web panels under pure shear, vol. 124; 1998 184–94 (no. 2).
- [16] Yoo CH, Lee SC. Mechanics of web panel postbuckling behavior in shear, vol. 132; 2006 1580–9 (no. 1).
- [17] Wagner H. Flat sheet metal girder with very thin metal web. Tech. Notes, 604, 605, 606. Washington, DC: National Advisory Committee on Aeronautics; 1931.
- [18] American Association of State Highway and Transportation Officials. AASHTO LRFD bridge design specifications 6th Edition; 2012 ([Online]. Available: <http://www.knovel.com/knovel2/Toc.jsp?BookID=4852>). [Accessed 13 February 2013].
- [19] White DW, Barker MG. Shear resistance of transversely stiffened steel I-girders. *J Struct Eng* 2008;134(9):1425–36.
- [20] Basler K. Strength of plate girders in shear. *Trans ASCE* 1961;128(2).
- [21] Gaylord EH. Discussion of K. Basler 'Strength of plate girders in shear'. *Trans ASCE* 1963;128(Part II):712.
- [22] Fujii T. On an improved theory for Dr. Basler's theory. *IABSE 8th Congr., Final Rep.*, New York; 1968.
- [23] Fujii T. On ultimate strength of plate girders. *Jpn Shipbuild Mar Eng* 1968;3(3):7–16.
- [24] Selberg A. On the shear capacity of girder webs. *Univ Trondheim Rep* 1973.
- [25] American Institute of Steel Construction. Steel construction manual. 14th ed.; 2011.
- [26] Porter DM, Rockey KC, Evans HR. The collapse behavior of plate girders loaded in shear. *Struct Eng* 1975;53(8):313–25.
- [27] Basler K, Yen BT, Mueller JA, Thurlimann B. Welded plate girders, report no. 251-13. Welded Plate Girder Project Committee; 1960.
- [28] European Committee for Standardization (CEN). Eurocode 1: Actions on structures – Part 1-2: General actions – actions on structures exposed to fire. Brussels: CEN; 2002.
- [29] Payá-Zaforteza I, Garlock M. A numerical investigation on the fire response of a steel girder bridge. *J Constr Steel Res* 2012;75:93–103 (Elvesier).
- [30] Selamet S, Garlock MEM. Plate buckling strength of steel wide-flange sections at elevated temperatures. *J Struct Eng ASCE* 2013;139(11):1853–65 (no. in press).
- [31] Elhami Khorasani N, Garlock M, Gardoni P. A Bayesian methodology for the performance evaluation of steel perimeter columns under fire. *11th International Conference on Structural Safety and Reliability*, New York; 2013.
- [32] Luecke WE, Banovic SW, McColskey JD. "High-temperature tensile constitutive data and models for structural steels in fire," NIST Technical Note 1714. United States of America: Department of Commerce; November 2011.
- [33] Lee SC, Lee DS, Yoo CH. Ultimate shear strength of long web panels. *J Constr Steel Res* 2008;64:1357–65.
- [34] Schiffler DC. Analysis of collapsed Alabama bridge due to fire. (M.S. Thesis) Princeton: Princeton University; 2011.
- [35] Alos-Moya J, Paya-Zaforteza I, Garlock MEM, Loma-Ossorio E, Schiffler D, Hospitaler A. Analysis of a bridge failure due to fire using computational fluid dynamics and finite element models. *Eng Struct* 2014;68:96–110.